Chemical Engineering Journal 446 (2022) 136827

Contents lists available at ScienceDirect

Chemical Engineering Journal

journal homepage: www.elsevier.com/locate/cej

In-situ constructing slow-release Li-Al-O interface layer for lithium metal batteries to enhance interface stability and suppress lithium dendrite growth

Dexuan Pei [a], Ziying Liu [a], Rui Ma [a], Shuo Huang [a], Shuen Hou [a], Min Liu [b], Guozhong Cao [c], Hongyun Jin [a,*]

[a] Engineering Research Center of Nano-Geomaterials of Ministry of Education, Faculty of Materials Science and Chemistry, China University of Geosciences, Wuhan 430074, China
[b] Department of Technology Centre of Dongfeng Motor Group Co. LTD, Wuhan 430058, China
[c] Department of Materials Science & Engineering, University of Washington, WA 98195, USA

ARTICLE INFO

Keywords:
Composite polymer electrolytes
Slow-release Li-Al-O interface layer
Interface stability
Li dendrites

ABSTRACT

Composite polymer electrolytes (CPEs) have shown extraordinary promise for use in all-solid-state lithium metal batteries (LMBs) because of their tunable merits in ionic conductivity and mechanical flexibility. Their practical application is however hindered by the poor interface stability and the uncontrollable Li dendrite formation. Addressing these two issues, we report an in-situ formed Li-Al-O interface layer between CPEs and Li metal anode by introducing Al_2O_3 nanoparticles in CPEs. X-ray photoelectron spectroscopy results indicated that the CPE-Al_2O_3 could slowly release Al atoms which react with Li metal to form the current Li-Al-O interface layer. We highlight that the Li-Al-O interface layer can stabilize lithium deposition/stripping over 1400 h in lithium symmetric batteries, and afford an impressive cycle life of 300 cycles in $LiFePO_4$-Li batteries with almost no capacity loss. The present findings demonstrate that in-situ constructing a slow-release Li-Al-O interface layer is an easy and effective approach to stabilize the solid electrolyte interface and suppress the Li dendrites growth. Furthermore, the obtained batteries show excellent cycling stability, indicating the strategy with in-situ formed CPEs shed light on improving the processability of fabrication of high-performance electrolytes.

1. Introduction

Lithium metal batteries (LMBs) have been considered as one of the most promising power sources for numerous applications such as consumer electronic products, energy storage devices, and electric-drive vehicles [1–3]. However, LMBs using liquid electrolytes usually suffer from unstable solid electrolyte interface (SEI) and safety issues associated with the high chemical reactivity of Li metal and the formation of irregular metallic Li electrodeposits [4–6]. LMBs with composite polymer electrolytes (CPEs) have attracted extensive attention as one of the most sought-after solutions due to their outstanding merits: (i) they are non-vaporizable and nonflammable, and (ii) they exhibit promising electrochemical stability and mechanical performance [7]. However, the poor CPEs/Li interface stability and the formation of lithium dendrites across the CPEs/Li surface in LMBs (i.e., inhomogeneous stripping and plating reaction of metallic lithium anode during cycling) hinder the practical application of CPEs in LMBs [8–11].

Many efforts have been made to address these issues, such as constructing an artificial SEI layer, which is considered to be an effective method to stabilize the CPEs/Li interface [12,13]. Huang et al. in situ constructed a Li_3N layer between electrolyte and Li anode, which enhanced the interfacial stability [14]. Hu et al. made a Li-rich artificial SEI layer in the PEO-based CPEs, which improved the cycle performance in batteries [15]. Among the artificial interface layers, the thermodynamically stable Li-Al-O interface was created to reduce the contact resistance and increase the interface stability between CPEs and Li metal anode [16]. Therefore, many efforts have been made to construct the Li-Al-O interface. Huang et al. synthesized a polycrystalline Li-Al-O electrolyte via chemical reaction aiming to protect the Li anode and elongated the cycle life of Li symmetric batteries. But the electrolyte consisted of complex composition, and the Li-AL-O electrolyte lacked of flexibility [17]. Chen et al. constructed a Li-Al-O composition through

* Corresponding author.
E-mail address: jinhongyun@cug.edu.cn (H. Jin).

https://doi.org/10.1016/j.cej.2022.136827

Available online 7 May 2022

an in-situ sol-gel method, which exhibited fast Li-ion transport and good dendrite suppression capability. However, the existence of ionic liquid decreased the mechanical strength of the CPEs, which may affect the safety of the battery [18]. Jing et al. dispersed Al_2O_3 fillers into a PPC-based polymer matrix with graphite coating procedure, in which an interface layer composed of Li-Al-O and LiC_6 was formed, and the cycling performance in symmetric Li batteries was improved. But it was also unclear whether the performance improvement mainly comes from LiC_6 or Li-Al-O [19]. Especially, these methods are difficult to be implemented to a large-scale promotion for commercial applications since some toxic solvents are inevitably used. Therefore, it is highly desired to construct a Li-Al-O layer in a simple and environment-friendly way to improve the cycle stability and suppress the Li dendrites in CPEs.

In this study, we introduce nano Al_2O_3 fillers into the PCL matrix through a simple solution casting method, aiming to in-situ construct a Li-Al-O interface between CPEs and the Li metal anode during LMBs cycling. The composition and morphology of the interface layer are revealed by X-ray photoelectron spectroscopy (XPS) and scanning electron microscope (SEM) characterizations. We highlight that the symmetric Li/CPEs/Li batteries and LFP/CPEs/Li batteries exhibit excellent cycle stability due to the formation of the slow-release Li-Al-O interface layer on the Li metal anode.

2. Experimental

2.1. Material preparation

Commercially available Aluminum oxide (γ-Al_2O_3, 10 nm, Aladdin, 99.99%) with an average diameter of 9.8 nm was shown in **Figure S1**. Polycaprolactone (PCL) with the weight average molecular weight (M_w) of 56128 g·mol^{-1}, and a PDI of 1.98 were obtained by the gel permeation chromatography (GPC) measurement (**Figure S2**, Table S1). Bis-trifluoromethanesulfonimide lithium salt (LITFSI, Macklin, 99.9%), Dimethyl carbonate (DMC, Aladdin, 99%), and Ferrous lithium phosphate ($LiFePO_4$, Tianjin STL Energy Technology) were commercially obtained. In addition, the PCL, and Al_2O_3 are dried in a vacuum oven for 12 h.

2.2. Preparation of CPEs

The condition of preparation of CPEs were shown in **Figure S3**. CPEs were prepared by a solution casting procedure [20]. The PCL and nano Al_2O_3 fillers were dried in a vacuum drying oven for 12 h to remove the absorbed water from the atmosphere. Then the PCL and LITFSI in an optimized mole ratio of 20:1 were dissolved in 15 mL DMC (Aladdin, 99%) solution and continuously stirred at 60 °C for 2 h [21]. Then different amounts of nano Al_2O_3 with contents of 0%-30% were added. The solution was finally mixed for 24 h with continuous heating. Especially, during the stirring process, the solution was ultrasonic dispersed per 2 h. The solution was cast on a glass plate using a doctor blade when a significant homogenization has taken place. Residual solvent was completely removed by drying the electrolyte film in a vacuum oven at room temperature for another 24 h. The thickness of CPEs was controlled at about 50–60 μm. For electrochemical tests, the obtained CPEs membranes were cut into circular rounds with a diameter of 19 mm and placed in an Ar-filled glove box for overnight to remove the residual solvent. For simplification, CPEs with different amounts (0–30%) of nano Al_2O_3 were denoted as CPE-A0, CPE-A10, CPE-A20, and CPE-A30, respectively.

2.3. Sample characterization

The crystal structure was determined by a D8-ADVANCE X-ray diffractometer (XRD) using Cu K_α radiation. The morphology and microstructure of CPEs were studied by scanning electron microscopy (SEM, HITACHI SU8010). X-ray photoelectron spectroscopy (XPS) was measured utilizing the Thermo Scientific K-Alpha system to measure elemental species and the chemical valence of the CPEs.

2.4. Electrochemical characterization

Coin cells SS/CPEs/SS (SS, stainless-steel plate electrodes) were assembled to determine the ionic conductivity(σ) of the CPEs by alternating current (AC) impedance measurements over the frequency range 10 MHz to 0.1 Hz with a potential amplitude of 10 mV using a Zahner electrochemical workstation. The value of σ of the CPEs can be calculated by Eq. (1) [22]:

$$\sigma = L/RS \tag{1}$$

where L is the thickness of the electrolyte membrane, R represents the impedance of the symmetrical stainless blocking batteries and S is the electrode area. Coin cells Li/CPEs/SS were assembled to measure the electrochemical window of CPEs by linear sweep voltammetry (LSV) technique at a scanning rate of 0.1 mV·s^{-1} using CHI660E. The Li-ion transference number(t_{Li+}) can be calculated by the Bruce-Vincent formula in Eq. (2) [23]:

$$t_{Li+} = \frac{I_s(\Delta V - I_0R_0)}{I_0(\Delta V - I_SR_S)} \tag{2}$$

where I_0 and I_s represent the initial and stable current obtained from the DC polarization curves of symmetrical Li/CPEs/Li battery (ΔV = 10 mV), respectively. R_0 and R_s correspond to the impedance before and after polarization, respectively. The galvanostatic test of both Li/CPEs/Li batteries and $LiFePO_4$/CPEs/Li full solid-state batteries were carried out on a Land battery testing system at 60 °C.

3. Results and discussion

It is reported that a loose layer consisting of LiF and CF_3-containing layer may form between CPEs and Li metal anode during cycling [24]. The formation process of a Li-Al-O interface in CPE-A20 is illustrated in **Fig. 1**. The Al_2O_3 nanoparticles in the CPEs are expected to slowly release Al atoms and react with Li metal to form a Li-Al-O interface layer between CPEs and Li metal anode during battery cycling. This interface layer is expected to stabilize the CPEs/Li interface and make a uniform Li deposits process over the Li surface, as well as suppress the Li dendrite growth.

To verify whether a Li-Al-O interface layer is formed between the CPE-A20 and the Li metal anode during battery cycling, we characterized the Li electrode before and after 10 cycles in LFP/CPE-A20/Li battery through XPS. **Fig. 2(a)** shows the full XPS spectra on the Li surface before and after 10 cycles. Both Li surfaces before and after 10 cycles in LFP/CPE-A20/Li battery contained C, O, and F. It was worth noting that in the F1s spectrum, peaks at 684.6 and 688.7 eV (**Figure S4**) were assigned to LiF and CF_3. The LiF and CF_3 originated from the decomposition of lithium salts. After 10 cycles, Al existed on the Li surface after cycling in LFP/CPE-A20/Li battery, indicating the slow release of Al atoms during cycling in batteries. The deconvolution of the Al2p peak, as shown in Fig. 2**(b, c)**, was fitted with two peaks at 75.1 and 73.6 eV, corresponding to γ-Al_2O_3 [19] and Li_xAlO_y [18], respectively. The obtained results indicated the formation of the Li-Al-O compound on the Li surface. And the formation process of the Li-Al-O interface can be concluded as follows: Al_2O_3 nanoparticles exposed on the interface between the Li metal anode and CPEs electrolyte are prone to react with Li to form a stable Li-Al-O composition spontaneously during charging/discharging. Then slow released Al atoms continue to react with Li metal during cycling. And Li atoms could be delivered by this interface layer to the CPEs while maintaining this structure.

The corresponding raw materials, i.e., CPEs, were characterized through XRD, SEM, and EDS, and the obtained results were shown in **Figure S5**. Then the electrochemical performances of the CPEs were

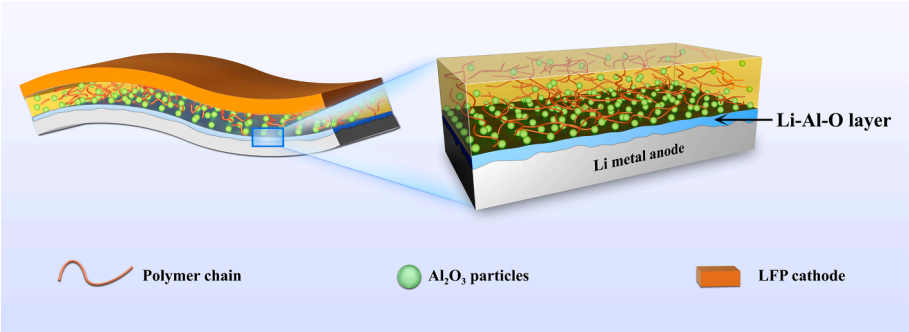

Fig. 1. The schematic illustration of in situ forming Li-Al-O interface layer and the inhibition of Li dendrites in the CPE-A20.

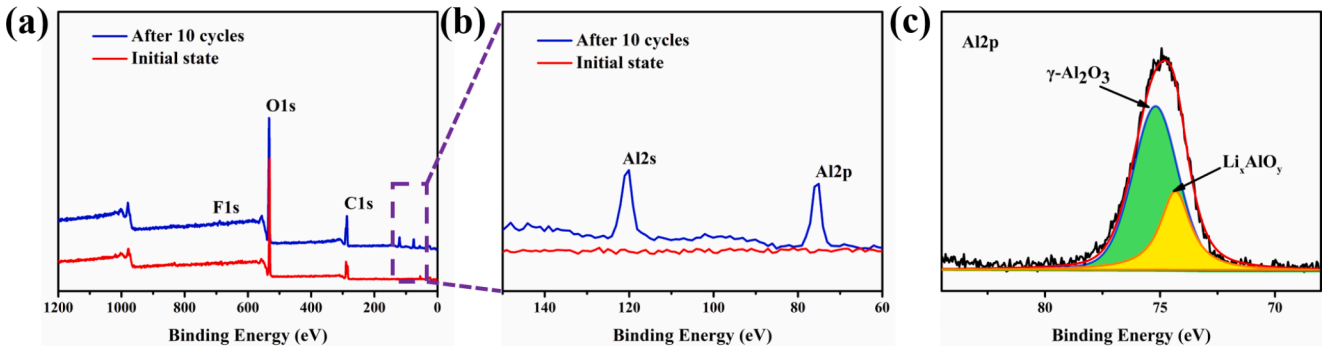

Fig. 2. Full XPS spectra of (a, b) the initial state of Li surface and after 10 cycles in LFP/CPE-A20/Li battery. (c) XPS spectra of Al2p of CPE-A20 after 10 cycles in LFP/CPE-A20/Li battery.

characterized. In Fig. 3**(a, b)**, the ionic conductivities of CPEs membranes at different temperatures (from 30 to 60 °C) were presented. The σ of CPE-A0 was only 6.32 × 10^{-6} S·cm^{-1}. After Al_2O_3 nanoparticles adding to the CPEs, the σ increased firstly as the σ reached to 1.72 × 10^{-5} S·cm^{-1} for CPE-A10 and 1.94 × 10^{-5} S·cm^{-1} for CPE-A20 at 60 °C. When the content of Al_2O_3 reached to 30%, the σ decreased to 1.23 × 10^{-5} S·cm^{-1}, which may be ascribed to that excess Al_2O_3 nanoparticles likely to agglomerate, leading to the elimination of effective interaction interfaces as well as the lowering of polymer free-volume [25]. Therefore, the conductivity in turn decreased. The LSV measurements from 1.0 to 7.0 V at 0.1 mV s^{-1} were carried out, and the obtained results were shown in Fig. 3**(c)**. The CPEs membranes were relatively stable below approximately 6.0 V (*vs* Li/Li^+). The calculated Li-ion transference number (t_{Li+}) was shown in Fig. 3**(d)**. CPE-A20 had a t_{Li+} value of 0.65 at 60 ℃, and the t_{Li+} value of CPE-A10 and CPE-A30 are 0.56, and 0.51 (**Figure S6**), respectively. These results showed that CPEs with Al_2O_3 nanoparticles exhibited a relatively high t_{Li+}, which could mean a good battery property for the CPEs.

Cycling performance heavily relied on the electrode/electrolyte interface stability. Here we investigated the battery cycle performance of LFP/CPEs/Li to further assess the interface stability. The rate performance and charge/discharge profiles of CPEs were shown in **Figure S7**, respectively. The LFP/CPE-A20/Li battery delivered the specific capacities of 140.7, 135.1, 127.4, 121.3 and 118.1 mAh·g^{-1} at different discharge rates of 0.1, 0.2, 0.5, 0.8 and 1.0C, respectively. And the specific capacities of LFP/CPE-A30/Li battery were 128.6, 122.9, 110.9, 105.7 and 100.0 mAh·g^{-1} at the same rate. Note that LFP/CPE-A20/Li and LFP/CPE-A30/Li batteries showed the initial capacity of 120.7 and 102.4 mAh·g^{-1}, and both of them exhibited outstanding capacity retention of 98% and 100%, after 300cycles at 1.0C, as shown in Fig. 4 **(a, b)**. The excellent cycle stability for the LFP/CPE-A20/Li and LFP/CPE-A30/Li batteries might originate from the in-situ Li-Al-O interface layer, which facilitated interfacial charge transport, and shorten the ion diffusion pathway [26]. However, the LFP/CPE-A10/Li battery suffered from a sudden capacity fading, this might come from the poor thermal stability for CPE-A10 because of the low content of Al_2O_3 nanoparticles [27]. The thermal shrinkage properties of the CPEs were investigated as shown in **Figure S8**. It should be mentioned that the battery performance of the present CPE-Al_2O_3 compares favorably with many reported CPEs (Table S2). As a result, the excellent cycle stability of the LFP/CPE-A20/Li and LFP/CPE-A30/Li batteries indicated that a slow-release Li-Al-O interface layer was formed and this interface layer was concluded to be responsible to enhance the battery performance.

SEM images of the cross-section of the LFP/CPE-A20/Li battery after cycles was shown in **Figure S9(a)**. There was no obvious boundary between the electrolyte and electrodes, indicating a tight integration. The morphology of Li metal anode before cycling was shown in **Figure S9(b)**. For the Li metal anode with CPE-A20 and CPE-A30 at 1.0C in LFP/CPE/Li batteries after 300cycles, a flat and compact surface morphology was observed (Fig. 4**(c-f)**) with packed and plate-like Li, indicating a uniform and stable lithium deposits during cycling. Furthermore, the Li-Al-O interface layer could ameliorate the intimate contact between the electrolyte and electrode and promote the lithium ions transport, thus obtaining a smooth surface structure on the Li metal anode. Moreover, no Li dendrites can be observed on the surface of the Li metal anode, which suggested the Li-Al-O interface layer was favorable to inhibit Li dendrites penetration. The results indicated that the slow-release Li-Al-O interface layer effectively improved the stability of the CPEs/Li interface and significantly inhibited the formation and growth of lithium dendrites on the surface of lithium metal.

Lithium stripping and plating experiments were further performed to analyze the cycling stability of the CPE-A20 and CPE-A30 against lithium metal. The lithium plating/stripping cycling in the Li/CPE-A20/Li, and Li/CPE-A30/Li symmetric batteries at different current densities from 0.01 to 0.2 mA·cm^{-2} were shown in **Figure S10**. Both CPE-A20 and CPE-A30 in symmetric batteries exhibited stable rate performances until the current up to 0.2 mA·cm^{-2}. To further investigate the cycle stability

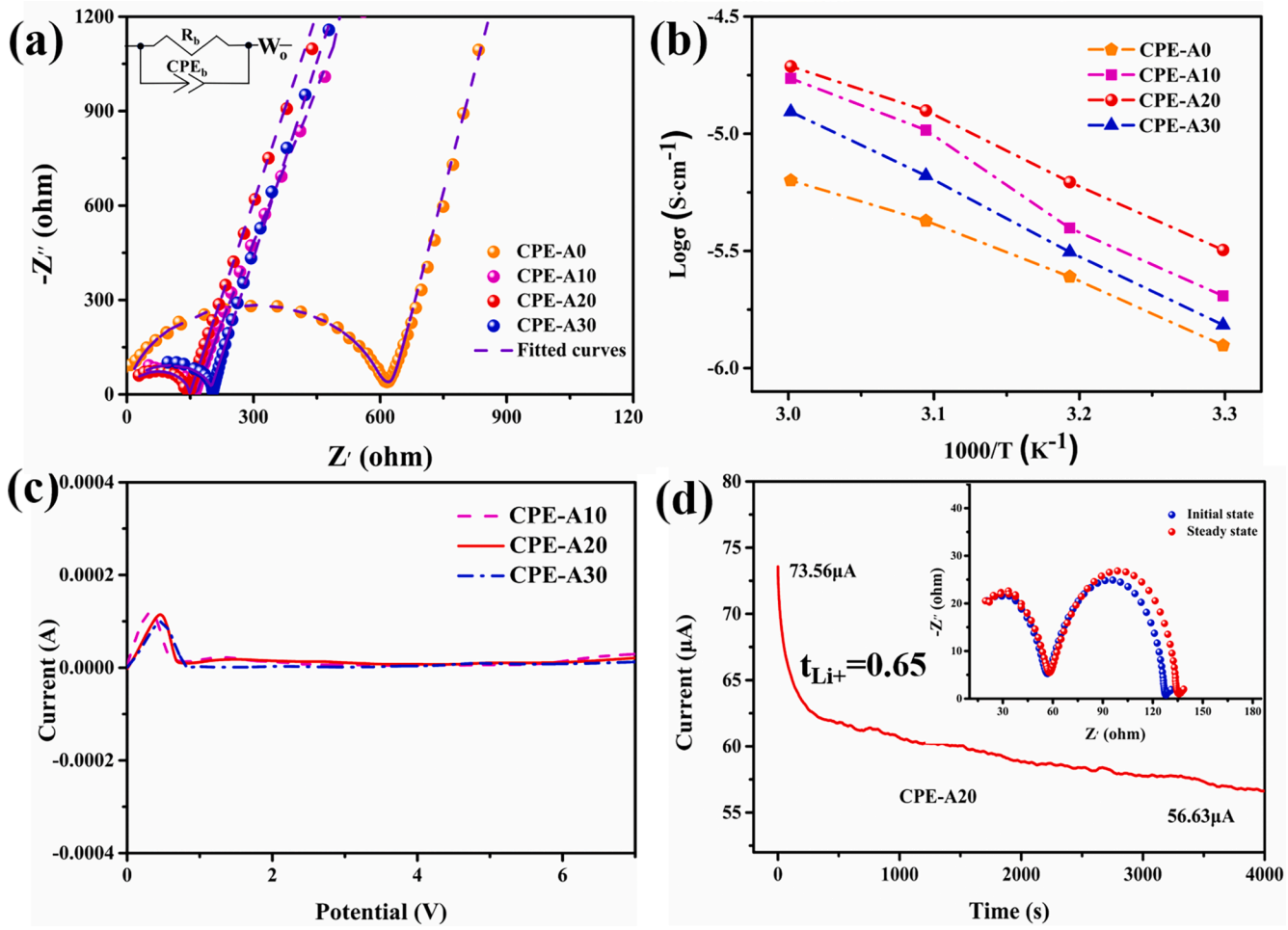

Fig. 3. (a) Impedance plots of the CPEs at 60 ℃, (b) Arrhenius plots for the ionic conductivity of the CPEs. (c) LSV curves of CPEs and (d) steady state polarization curve and the impedances of the Li/CPE-A20/Li battery before and after polarization.

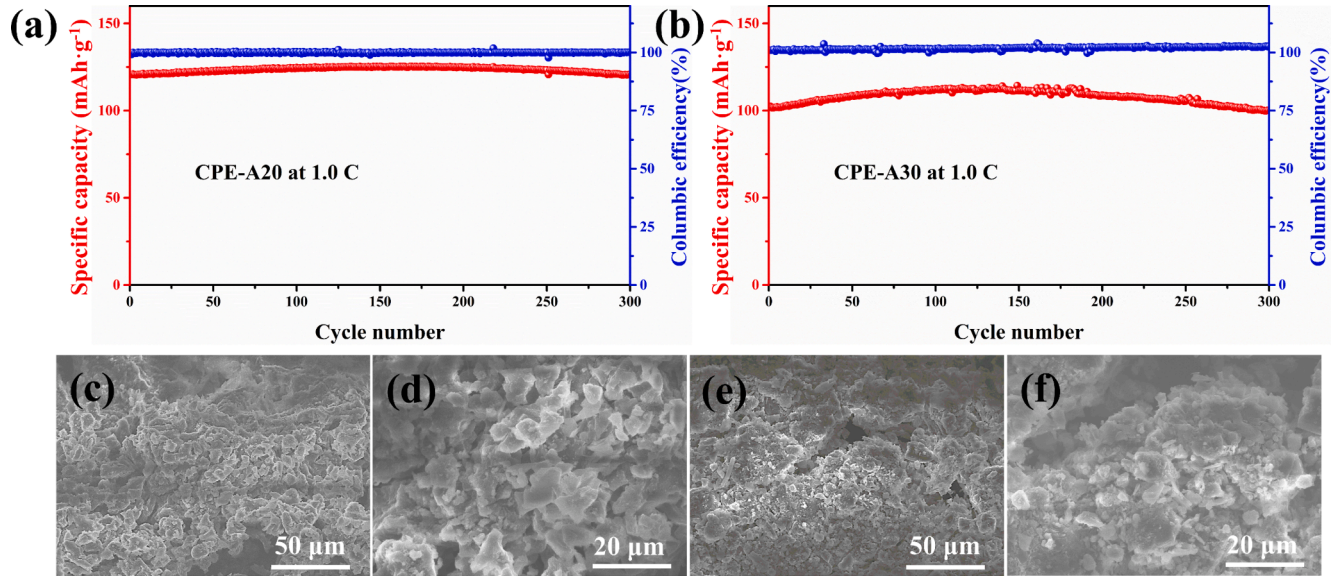

Fig. 4. Cycle performance of (a) LFP/CPE-A20/Li and (b) LFP/CPE-A30/Li batteries. SEM images of Li surface after 300 cycles in (c, d) LFP/CPE-A20/Li battery and LFP/CPE-A30/Li battery, respectively.

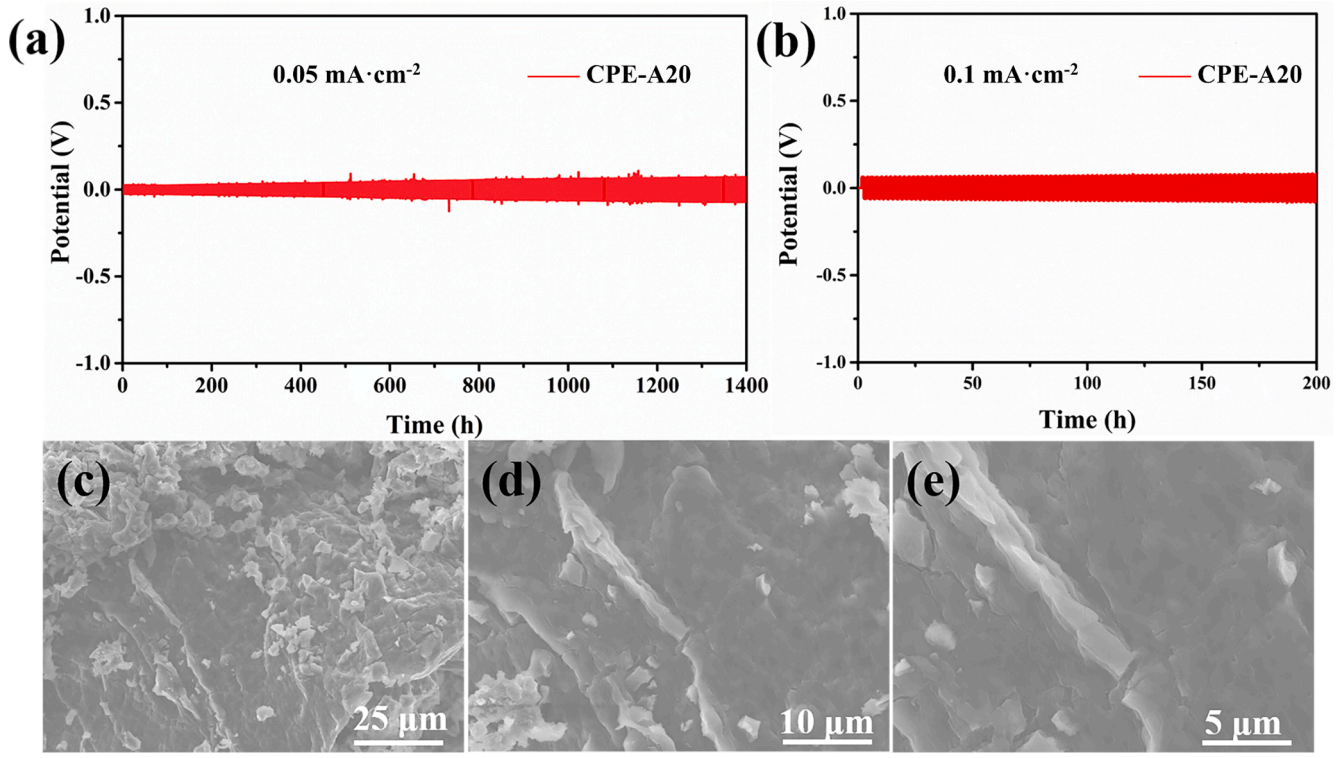

Fig. 5. Lithium stripping/plating cycle tests of Li/CPE-A20/Li symmetrical batterie at (a) 0.05 mA·cm^{-2} and (b) 0.1 mA·cm^{-2}. (c-e) SEM images of Li surface after cycling in Li/CPE-A20/Li symmetrical battery after 1400 h at 0.05 mA·cm^{-2}.

between the CPEs with Li metal, the galvanostatic lithium stripping and plating measurements were carried out at 60 ℃ at 0.05 mA·cm^{-2}. As shown in Fig. 5**(a),** the CPE-A20 showed a stable voltage initially, suggesting an interface formed between electrolytes and Li metal anode [28]. Especially, the Li/CPE-A20/Li battery can be charged and discharged for over 1400 h with a small voltage polarization of about 0.071 V at 0.1 mA·cm^{-2}, and about 0.083 V after 200 h at 0.1 mA·cm^{-2}, as shown in Fig. 5**(b)**. Similar phenomenon was shown in Li/CPE-A30/Li battery shown in **Figure S11**, as the voltage polarization is about 0.046 V at 0.05 mA·cm^{-2} after 500 h and 0.124 V after 200 h at 0.1 mA·cm^{-2}. Such high stability of Li/CPE-A20/Li battery even after 1400 h cycles indicated that the addition of nano Al_2O_3 in PCL-based CPEs generated a more stable and higher quality Li-Al-O interface layer. Though a few vibrations appeared in the voltage profile in Li/CPE-A20/Li symmetric battery, the battery maintained a stable overpotential in the following cycles, indicating no uncontrolled increase of resistance caused by the degradation of the Li-Al-O interface layer on the Li metal anode [29]. The impedance associated with time in symmetric Li batteries was calculated. It is clear from Table S3 that the CPE-A20 and CPE-A30 showed stable impedance during cycling, which indicated that the Li-Al-O interface layer could greatly improve the Li stripping/plating stability in Li symmetric batteries. This explained why the cycle performances of CPE-A20 and CPE-A30 in the symmetric battery were stable.

To further explore the interfacial stability of Li-Al-O between the CPE-A20 and Li metal anode, and the inhibition of Li dendrites, we disassembled the cycled symmetric batteries to observe the Li/CPE-A20 interfaces. Fig. 5**(c-e)** shows SEM images of Li surface after cycling in Li/CPE-A20/Li symmetrical battery and the related images for CPE-A30 was shown in **Figure S12**. Although LITFSI salt has been previously reported to form a poor-quality SEI layer on Li metal anode [30], it is found that a relatively smooth and dense Li anode surface can be observed with rare Li dendrites after cycling in Li/CPE-A20/Li battery. A similar phenomenon is shown in **Figure S12** for the Li surface in Li/CPE-A30/Li battery after cycling. The smooth and dense surface of Li metal may be attributed to the in-situ formed slow-release Li-Al-O interface layer on the Li metal surface [31]. From the above analysis of both symmetric batteries and full batteries, the Li-Al-O interface layer can effectively improve the cycle stability and inhibit the Li dendrites.

4. Conclusions

In summary, a Li-Al-O interface layer was in-situ formed between Al_2O_3-based CPEs and Li anode during battery cycling. The formation of the Li-Al-O interface layer resulted from the reaction between the slowly released Al atoms and the Li metal anode. Benefiting from the stabilized Li-Al-O interface layer, the symmetrical battery with CPEs-Al_2O_3 electrolyte can be cycled over 1400 h with a small voltage polarization of ~ 0.071 V. Besides, excellent capacity retention reaching ~ 100% can be achieved in LFP/CPE-A20/Li batteries after 300cycles at 1.0C. The remarkable results confirmed the effectiveness of the in-situ formed Li-Al-O interface layer in improving the interfacial stability between CPEs and Li metal anode. SEM and XPS characterizations confirmed a smooth and stable Li-Al-O interface layer even after 1400 h in Li symmetric batteries and 300cycles in $LiFePO_4$-Li batteries. Our work provided a facile and effective strategy to stabilize the electrode/electrolyte interface and suppress the Li dendrite growth in LMBs.

Declaration of Competing Interest

The authors declare that they have no known competing financial interests or personal relationships that could have appeared to influence the work reported in this paper.

Acknowledgments

This work was financially supported by the National Natural Science Foundation of China (12192213), the Key Research and Development Program of Hubei (2021BAA175), and Major scientific and technological innovation in Hubei (2019AAA004).

Appendix A. Supplementary data

Supplementary data to this article can be found online at https://doi.org/10.1016/j.cej.2022.136827.

References

[1] S.M. Zhang, H.T. Gu, H.G. Pan, S.H. Yang, W.B. Du, X. Li, M.X. Gao, Y.F. Liu, M. Zhu, L.Z. Ouyang, D.C. Jian, F. Pan, A novel strategy to suppress capacity and voltage fading of li- and mn-rich layered oxide cathode material for lithium-ion batteries, Adv. Energy Mater. 7 (6) (2017) 1601066, https://doi.org/10.1002/aenm.201601066.

[2] T. Deng, L.S. Cao, X.Z. He, A.M. Li, D. Li, J.J. Xu, S.F. Liu, P.X. Bai, T. Jin, L. Ma, M. A. Schroeder, X.L. Fan, C.S. Wang, In situ formation of polymer-inorganic solid-electrolyte interphase for stable polymeric solid-state lithium-metal batteries, Chem 7 (11) (2021) 3052–3068, https://doi.org/10.1016/j.chempr.2021.06.019.

[3] C.W. Ma, C.C. Liu, Y.X. Zhang, X.Y. Zhang, Z.K. Zhao, T.L. Song, B.R. Wu, D.B. Mu, A dual lithiated alloy interphase layer for high-energy-density lithium metal batteries, Chem. Eng. J. 434 (2022), 134637, https://doi.org/10.1016/j.cej.2022.134637.

[4] C.L. Wei, Y.C. Zhang, Y. Tian, L.W. Tan, Y.L. An, Y. Qian, B.J. Xi, S.L. Xiong, J. K. Feng, Y.T. Qian, Design of safe, long-cycling and high-energy lithium metal anodes in all working conditions: Progress, challenges and perspectives, Energy Storage Mater. 38 (2021) 157–189, https://doi.org/10.1016/j.ensm.2021.03.006.

[5] G.L. Cui, Reasonable design of high-energy-density solid-state lithium-metal batteries, Matter 2 (4) (2020) 805–815, https://doi.org/10.1016/j.matt.2020.02.003.

[6] C.P. Yang, K. Fu, Y. Zhang, E. Hitz, L.B. Hu, Protected lithium-metal anodes in batteries: from liquid to solid, Advanced Matertials 29 (36) (2017) 1701169, https://doi.org/10.1002/adma.201701169.

[7] P. Fan, H. Liu, V. Marosz, N.T. Samuels, S.L. Suib, L.Y. Sun, L.B. Liao, High Performance Composite Polymer Electrolytes for Lithium-Ion Batteries, Advanced Functional Matertials 31 (23) (2021) 2101380, https://doi.org/10.1002/adfm.202101380.

[8] X.F. Wang, C.K. Fu, Z.J. Feng, H. Huo, X.C. Yin, G.L. Gao, G. Yin, L.J. Ci, Y.J. Tong, Z.X. Jiang, J.J. Wang, Flyash/polymer composite electrolyte with internal binding interaction enables highly-stable extrinsic-interfaces of all-solid-state lithium batteries, Chem. Eng. J. 428 (2022), 131041, https://doi.org/10.1016/j.cej.2021.131041.

[9] Q.Y. Guo, F.L. Xu, L. Shen, Z.Y. Wang, J. Wang, H. He, X.Y. Yao, Poly(ethylene glycol) brush on $Li_{6.4}La_3Zr_{1.4}Ta_{0.6}O_{12}$ towards intimate interfacial compatibility in composite polymer electrolyte for flexible all-solid-state lithium metal batteries, J. Power Sources 498 (2021), 229934, https://doi.org/10.1016/j.jpowsour.2021.229934.

[10] D.X. Cao, X. Sun, Q. Li, A. Natan, P.Y. Xiang, H.L. Zhu, Lithium dendrite in all-solid-state batteries: growth mechanisms, Suppression Strategies, and Characterizations, Matter 3 (1) (2020) 57–94, https://doi.org/10.1016/j.matt.2020.03.015.

[11] H.Y. Huo, Y. Chen, J. Luo, X.F. Yang, X.X. Guo, X.L. Sun, Rational design of hierarchical "ceramic-in-polymer" and "polymer-in-ceramic" electrolytes for dendrite-free solid-state batteries, Adv. Energy Mater. 9 (17) (2019) 1804004, https://doi.org/10.1002/aenm.201804004.

[12] Y. Wang, Y. Liu, Y. Tu, Q. Wang, Reductive decomposition of solvents and additives toward solid-electrolyte interphase formation in lithium-ion battery, The Journal of Physical Chemistry C 124 (17) (2020) 9099–9108, https://doi.org/10.1021/acs.jpcc.9b10535.

[13] Y. Chen, W.W. Li, C.Z. Sun, J. Jin, Q. Wang, X.D. Chen, W.P. Zha, Z.Y. Wen, Sustained release-driven formation of ultrastable sei between li_6ps_5cl and lithium anode for sulfide-based solid-state batteries, Adv. Energy Mater. 11 (4) (2021) 2002545, https://doi.org/10.1002/aenm.202002545.

[14] Y. Huang, B. Chen, J. Duan, F. Yang, T. Wang, Z. Wang, W. Yang, C. Hu, W. Luo, Y. Huang, Graphitic carbon nitride (g-c_3n_4): an interface enabler for solid-state lithium metal batteries, Angew. Chem. Int. Ed. 59 (9) (2020) 3699–3704, https://doi.org/10.1002/anie.201914417.

[15] Y.X. Liu, R.Z. Hu, D.C. Zhang, J.W. Liu, F. Liu, J. Cui, Z.P. Lin, J.S. Wu, M. Zhu, Constructing Li-rich artificial sei layer in alloy-polymer composite electrolyte to achieve high ionic conductivity for all-solid-state lithium metal batteries, Adv. Mater. 33 (11) (2021) 2004711, https://doi.org/10.1002/adma.202004711.

[16] L. Chen, J.G. Connell, A. Nie, Z. Huang, K.R. Zavadil, K.C. Klavetter, Y. Yuan, S. Sharifi-Asl, R. Shahbazian-Yassar, J.A. Libera, A.U. Mane, J.W. Elam, Lithium metal protected by atomic layer deposition metal oxide for high performance anodes, J. Mater. Chem. A 5 (24) (2017) 12297–12309, https://doi.org/10.1039/C7TA03116E.

[17] M.L. Xie, X. Lin, Z.M. Huang, Y.Y. Li, Y. Zhong, Z.X. Cheng, L.X. Yuan, Y. Shen, X. Lu, T.Y. Zhai, Y.H. Huang, A Li-Al-O solid-state electrolyte with high ionic conductivity and good capability to protect li anode, Adv. Funct. Mater. 30 (7) (2020) 1905949, https://doi.org/10.1002/adfm.201905949.

[18] Z.Y. Wen, Y.J. Li, Z.K. Zhao, W.J. Qu, N. Chen, Y. Xing, Y. Ma, L. Li, F. Wu, R. J. Chen, A leaf-like Al_2O_3-based quasi-solid electrolyte with a fast Li^+ conductive interface for stable lithium metal anodes, J. Mater. Chem. A 8 (15) (2020) 7280–7287, https://doi.org/10.1039/D0TA02098B.

[19] X.Y. Hu, M.X. Jing, H. Yang, Q.Y. Liu, F. Chen, W.Y. Yuan, L. Kang, D.H. Li, X. Q. Shen, Enhanced ionic conductivity and lithium dendrite suppression of polymer solid electrolytes by alumina nanorods and interfacial graphite modification, J. Colloid Interface Sci. 590 (2021) 50–59, https://doi.org/10.1016/j.jcis.2021.01.018.

[20] X. Li, D.H. Wang, H.C. Wang, H.F. Yan, Z.L. Gong, Y. Yang, Poly(ethylene oxide)-$Li_{10}SnP_2S_{12}$ composite polymer electrolyte enables high-performance all-solid-state lithium sulfur battery, ACS Appl. Mater. Interfaces 11 (25) (2019) 22745–22753, https://doi.org/10.1021/acsami.9b05212.

[21] D.X. Pei, R. Ma, G. Yang, Y.H. Li, C. Huang, Z.Y. Liu, S. Huang, H.Y. Jin, G.Z. Cao, Enhanced Ion transport behaviors in composite polymer electrolyte: the case of looser chain folding structure, J. Mater. Chem. A 10 (6) (2022) 3226–3232, https://doi.org/10.1039/D1TA10669D.

[22] Y. Nikodimos, L.H. Abrha, H.H. Weldeyohannes, K.N. Shitaw, N.T. Temesgen, B. W. Olbasa, C.J. Huang, S.K. Jiang, C.H. Wang, H.S. Sheu, S.H. Wu, W.N. Su, C. C. Yang, B.J. Hwang, A new high-Li^+-conductivity Mg-doped $Li_{1.5}Al_{0.5}Ge_{1.5}(PO_4)_3$ solid electrolyte with enhanced electrochemical performance for solid-state lithium metal batteries, J. Mater. Chem. A 8 (48) (2020) 26055–26065, https://doi.org/10.1039/D0TA07807G.

[23] D. Cai, D.H. Wang, Y.J. Chen, S.Z. Zhang, X.L. Wang, X.H. Xia, J.P. Tu, A highly ion-conductive three-dimensional LLZAO-PEO/LiTFSI solid electrolyte for high-performance solid-state batteries, Chem. Eng. J. 394 (2020), 124993, https://doi.org/10.1016/j.cej.2020.124993.

[24] X.Y. Ni, T. Qian, X.J. Liu, N. Xu, J. Liu, C.L. Yan, High lithium ion conductivity lif/go solid electrolyte interphase inhibiting the shuttle of lithium polysulfides in long-life li-s batteries, Adv. Funct. Mater. 28 (13) (2018) 1706513, https://doi.org/10.1002/adfm.201706513.

[25] X.X. Wu, K.Y. Chen, Z.G. Yao, J.L. Hu, M.S. Huang, J.W. Meng, S.P. Ma, T. Wu, Y. H. Cui, C.L. Li, Metal organic framework reinforced polymer electrolyte with high cation transference number to enable dendrite-free solid state Li metal conversion batteries, J. Power Sources 501 (2021), 229946, https://doi.org/10.1016/j.jpowsour.2021.229946.

[26] Y.L. An, Y. Tian, Y.C. Zhang, C.L. Wei, L.W. Tan, C.H. Zhang, N.X. Cui, S.L. Xiong, J.K. Feng, Y.T. Qian, Two-dimensional silicon/carbon from commercial alloy and co_2 for lithium storage and flexible $Ti_3C_2T_x$ MXene-based lithium-metal batteries, ACS Nano 14 (12) (2020) 17574–17588, https://doi.org/10.1021/acsnano.0c08336.

[27] T.K.J. Köster, L.V. Wüllen, Cation-anion coordination, ion mobility and the effect of Al_2O_3 addition in PEO based polymer electrolytes, Solid State Ionics 181 (11) (2010) 489–495, https://doi.org/10.1016/j.ssi.2010.02.005.

[28] Q. Pan, D.M. Smith, H. Qi, S. Wang, C.Y. Li, Hybrid electrolytes with controlled network structures for lithium metal batteries, Adv. Mater. 27 (39) (2015) 5995–6001, https://doi.org/10.1002/adma.201502059.

[29] X. Judez, G.G. Eshetu, I. Gracia, P. López-Aranguren, J.A. González-Marcos, M. Armand, L.M. Rodriguez-Martinez, H. Zhang, C. Li, Understanding the role of nano-aluminum oxide in all-solid-state lithium-sulfur batteries, ChemElectroChem 6 (2) (2019) 326–330, https://doi.org/10.1002/celc.201801390.

[30] Q. Ma, X. Qi, B. Tong, Y. Zheng, W. Feng, J. Nie, Y.S. Hu, H. Li, X. Huang, L. Chen, Z. Zhou, Novel $Li[(CF_3SO_2)(n\text{-}C_4F_9SO_2)_N]$-based polymer electrolytes for solid-state lithium batteries with superior electrochemical performance, ACS Appl. Mater. Interfaces 8 (43) (2016) 29705–29712, https://doi.org/10.1021/acsami.6b10597.

[31] L. Somerville, J. Bareño, S. Trask, P. Jennings, A. McGordon, C. Lyness, I. Bloom, The effect of charging rate on the graphite electrode of commercial lithium-ion cells: A post-mortem study, J. Power Sources 335 (2016) 189–196, https://doi.org/10.1016/j.jpowsour.2016.10.002.